Telescope mirror supports: plate deflections on point supports

Jerry E. Nelson
Lawrence Berkeley Laboratory, Space Sciences Laboratory, University of California, Berkeley, California 94720
Jacob Lubliner
Department of Civil Engineering, University of California, Berkeley, California 94720
Terry S. Mast
Lawrence Berkeley Laboratory, Space Sciences Laboratory, University of California, Berkeley, California 94720

Abstract

We describe the deflections of uniform-thickness plates supported by discrete points and by continuous rings. The calculations are based on the theory of deflections of thin plates. In some cases the effect of shear on the deflections is also included. The optimum locations of the support points for a wide variety of simple geometries are given. The deflections and methods for estimating the deflections for the limiting case of a large number of support points are also described. Since the slope errors induced in a mirror by its support may be relevant to optical image quality, we describe a method of relating the surface deflections to the surface slopes, and hence the geometric optics image blur that results from a support system. These results are particularly useful for the support of very thin mirrors, where the optimum support is needed.

1. Introduction

One of the most challenging problems in the design and construction of large telescopes is that of properly supporting the primary mirror so that the large forces due to gravity do not objectionably alter its shape. High quality telescopes typically require that the mirror deformations be limited to some small fraction of the wavelength of light that the telescope is designed to use. For optical telescopes in particular, the deflection tolerances are sufficiently small that great care must be taken in the mirror support if these tolerances are to be met.

As a telescope points to different zenith angles the direction of gravity relative to the primary mirror changes. As a result of this, a mirror support system must be able to carry this force both in the axial direction (normal to the mirror surface) and in a radial direction (parallel to the mirror surface). These two components typically have different support systems, and it is often the case that the axial support is the more delicate and difficult support problem. For large mirrors this axial support is usually provided by some distribution of forces applied along the back side of the mirror, or at some points located along the center of gravity of the mirror. The radial support system is similar in form, typically being a system of forces applied either around the periphery of the mirror, or at discrete points located along the midplane of the mirror. In this paper we will not deal explicitly with the problems of radial support, but will only address the nature of axial supports. This general problem has been of great interest in the past, and a detailed study of axial support systems in theory and practice was made by Couder (1931). More recently, the entire field of the support and testing of astronomical mirrors was reviewed in a symposium (Crawford et al., 1968). Several specific mirror supports are also described by Pearson (1980).

The largest telescopes have used a discrete set of point supports for their axial support. The Soviet 6m telescope has 60 back supports, while the Hale 200" (5m) has 36 back supports, and smaller telescopes such as the Lick 3m have 18 back support points. These points of support are points at which specified forces are applied, often with counterweight systems. Other methods of applying these forces include air pads and whiffletree systems. In other cases, back support has been achieved by using ring supports with, for example, fluid filled tubes to achieve a uniform distribution of force along the circumferential length of the tubes.

Although axial supports for telescope mirrors have been dealt with in some detail by previous authors and telescope designers, the current desire to build extremely thin and large mirrors makes the subject of great interest. General design guidelines for possible supports of these very flexible mirrors will be most useful.

In addition, the recent interest in telescope mirrors that are segmented or composed of multiple telescope primaries, makes the uniformity of focal length a new and critical issue. With the support of only a single mirror concern over the accurate control of the radius of curvature of the mirror is minimal. In this case, changes in the focal length of the mirror due to imperfections in the support only require a refocusing of the telescope, something which is often required as a result of thermal effects in any case. For telescopes that have primaries with multiple mirror components, the focal lengths of the mirrors should either not change at all, or at least all change together. Particularly for segmented primaries, where one may attempt to accommodate both observations in the visible (seeing limited) and infrared (diffraction limited) regimes, all segments must have the same focal length to very high accuracy. Of course for the support of flats the proper control over the curvature is essential as well.

In section 2 we will develop some scaling laws and other semi-quantitative rules to aid in the conceptual design of axial support systems. In keeping with our concern over focal length, we will consider any plate deformations that alter the focal length as detrimental. A variety of examples of optimized support systems will also be given as further aid in the design of supports. Because the goals of this work are rather general, simple idealized cases are discussed, rather than specific realistic cases that must be dealt with in the detailed design of a specific support system. In this spirit we will typically ignore the effects of central holes, variable mirror thickness, shell effects, and the effects of shear in mirror deformation. Section 2 describes general scaling laws that apply to the deformation of thin plates. Section 3 discusses the deflection of plates that are infinite in extent. These have no edge effects and thus represent the limiting case of a mirror that is supported at a great many points. Section 4 gives for a variety of cases the optimized support configurations for circular plates. These cover both point supports and continuous ring supports. In the final section we briefly address the issue of support tolerances and sensitivity.

In keeping with the optical motivation for these studies, we evaluate the effect on the image quality of imperfections in the mirror support. There are two common ways of evaluating mirror distortions. 1) Using the geometric optics approximation the image blur is evaluated from slope errors in the mirror surface. 2) The other extreme characterizes the mirror surface by the root mean square deviation (rms) of the mirror from its desired shape, and thus characterizes the image by an rms wavefront error.

This approach assumes that the wavefront error can be characterized by a single number and that this determines the optical effects. Although this is an excellent approximation when the wavefront errors are small compared to the wavelength of light, and the geometric limit is a good approximation when the wavefront errors are large compared to the wavelength of light, the intermediate case requires the full and complex application of the physical theory of light. Some tools for understanding this intermediate region are contained in our report to this conference "The Effects of Mirror Segmentation on Telescope Image Quality (Mast et al.)." Conceivably the "optimum" support support will depend on which approach one chooses for analyzing image blur, but as we show in the next section, a fairly quantitative relation can be made between rms surface error and maximum slope errors, so both approaches should give essentially identical results. We typically will optimize on the rms surface deviation from the mean deflection rather than the slope errors. The peak-to-valley error is also closely related to the rms surface error. It is commonly the case that the peak-to-valley error is about five times the rms, and hence they are essentially equivalent. However, since the peak-to-valley only gives information from two extreme points, whereas the rms is averaged over the entire surface, the rms is normally the more useful surface characterization.

2. Scaling Laws

In the theory of thin plates where only flexural bending contributes to the plate deflection and shear effects are ignored, deflections of circular plates take the form:

$$\delta_{rms} = k\frac{qa^4}{D} \tag{1}$$

where

q = the applied force per unit area
a = the plate radius,
$D = Eh^3/12(1-\nu^2)$, the flexural rigidity,
E = the material elastic modulus,
ν = the material Poissons ratio,
h = the plate thickness, and
k is a parameter that depends on the nature of the support configuration.

For self-weight deflections this gives the well known scaling law that the deflections vary as:

$$\delta \backsim \frac{a^4}{h^2} \tag{2}$$

For non-circular plates a generalized form of this relation is more useful.

$$\delta_{rms} = \xi\frac{qA^2}{D} \sim \frac{A^2}{h^2}, \tag{3}$$

where A is the plate area and ξ, the support efficiency, is a dimensionless parameter that depends on the support configuration. This form is useful for estimating for example the deflections of hexagonal plates, a shape desired in segmented mirrors.

When one considers the deflection with N support points, it is evident that a pertinent parameter is the area per support point, rather than the area itself. Thus one can couch the rms deflection of a plate supported by N points in the following form:

$$\delta_{rms} = \gamma_N\frac{q}{D}\left(\frac{A}{N}\right)^2 \tag{4}$$

In this form, once γ_N is known, the deflection for a mirror of any size can be found.

The virtue of this form of the deflection law is that the parameter γ_N becomes a fixed constant for an optimized support configuration, at least in the limit of large N. For small values of N there will be noticeable edge effects that will make γ_N a function of the number of support points. As the number of support points increases γ_N will decrease to an asymptotic limit γ_∞. Improperly optimized support systems will of course have a larger γ than otherwise. Recognizing that γ is a measure of the efficiency of a given support configuration, we call γ the support point efficiency.

We will typically ignore the effects of shear. This eases the calculations and allows us to ignore the effects of plate thickness, except in D. However, a rough estimate of the additional deflections that will result from the inclusion of the effects of shear can be found by use of the formula

$$\delta_{total} = \delta_{bending}\left[1 + \alpha\left(\frac{h}{u}\right)^2\right] \tag{5}$$

where u is an effective length between support points, and α is a constant. If one defines u from the relation

$$N\pi u^2 = A \tag{6}$$

then for a variety of cases numerically evaluated one obtains an approximate value for α of $\alpha = 2$. Note that this rough formula only applies to plates that have optimized supports. A non-optimized support may have a much larger bending deflection but essentially the same shear deflection, and the inclusion of shear effects then results in a smaller change than indicated. We emphasize that the effects of shear scale according to the thickness-to-support-point span ratio, rather than according to the thickness-to-plate-radius ratio.

As mentioned earlier, the optical effects due to mirror deflections are often estimated using surface slopes rather than the rms deviation of the surface from its desired shape. The slope, the rms deflection, and the effective length must have at least a rough relationship,

$$S \sim \delta_{rms}/u \tag{7}$$

This gives the scaling relation of

$$S = g_N\frac{q}{D}\left(\frac{A}{N}\right)^{3/2} \quad \frac{1}{h^2}\left(\frac{A}{N}\right)^{3/2} \tag{8}$$

One can test these relations in a variety of cases to find a value for the parameter g. We have found for a surprising variety of cases that, for systems optimized to give the minimum rms deviation from the desired surface, the maximum slope can be found (within ~20%) by using

$$g_N = 9\gamma_N \tag{9}$$

The maximum image diameter is four times the maximum slope. Because of this well defined slope vs displacement relation, and because we are particularly interested in deflections that are sufficiently small to allow diffraction limited performance, we will characterize the surface by its rms deviation from the ideal one for the rest of the paper. This means that the average deflection on a given support system has been removed. We include all other effects including changes in the overall radius of curvature (focus).

3. Infinite Plates

Real finite plates have a variety of edge effects that tend to increase the plate deflections and appreciably complicate the analysis of their deflection. If a plate is simply supported

at many points, the deflections near a given support point will be dominated by the locations of the neighboring support points and will be only weakly effected by the location and shape of the free edge of the plate. For these reasons, infinite plates are worth studying. We also expect that no finite plate can be supported as efficiently as an infinite plate, thus, the efficiency coefficient for an infinite plate will set a lower bound on the efficiency coefficient of any point support system for a finite plate. Finally, the study of infinite plates can serve as a useful guide for the optimal topology of support point locations for finite plates.

If we restrict ourselves to point support grids that are identical for all support points,, only three topologies are possible. These are shown in Figure 1 and are the ones with three neighboring points (hexagonal), with four neighboring points (square), and one with six neighboring points (triangular). Because these support topologies are different, we expect that their efficiency coefficients will differ as well.

The deflections of an infinite plate supported by rectangular rows of support posts is a classic problem in plate theory. A discussion of this problem and its solution are given by Timoshenko (1959). This solution can be readily applied to the square grid case.

The deflections of the plate on triangular and hexagonal support point grids can also be readily found. Following an idea by Medwadowski (1981), we consider the deflections of a plate supported by a rectangular grid of support points and use the principle of linear superposition to find the triangular and hexagonal case deflections. Details of this derivation, and the results are given in Appendix A. The results for these grids can be summarized by determining γ as defined in Equation 4. We find

$$\gamma_{hexagonal} = 2.36 \times 10^{-3}$$
$$\gamma_{square} = 1.33 \times 10^{-3}$$
$$\gamma_{triangular} = 1.19 \times 10^{-3}$$

Note that these results are independent of Poissons ratio ν.

Not surprisingly, the triangular grid is the most efficient, and the hexagonal grid is decidedly the worst. It follows from this that the triangular grid is the basic topological pattern that should be used as a starting point in the optimization of support point forces and locations for finite plates.

4. Circular Plates

We now turn to the most common shape for primary mirrors, the circle. As mentioned before, we will not explicitly discuss annular plates or variable thickness plates, or include the effects of shear or the curvature of the plate. These effects should be included in any detailed analysis of a specific system. We will first discuss the deflections that result from point supports. We then evaluate deflections due to ring supports which for some configurations form a limiting case of point supports.

In analyzing and optimizing support systems in general, we strongly emphasize that the supports provide specified forces, but do not by themselves define the position of the mirror. In the case of N support points, three of these points can be specified to define the rigid body motion of the mirror, but the other support points should in practice be allowed to float in position and only provide the specified force. It follows from this that the deflections at the support points are not required to be zero for the overall optimized support. This is important in developing a physical intuition for these systems and differs markedly from the intuition one has of conventional supports of plates on fixed points.

To find the deflections of a circular plate supported by a series of points we will use the principle of superposition and divide the support points up into groups, each group containing k points uniformly spaced around a circle of a fixed radius as shown in Figure 2. The derivation for the deflections due to a single such group is given in Appendix B. The deflection has the form

$$w(\rho,\theta) = \sum_{m=0}^{\infty} w_m(\rho)\cos(km\theta) \qquad (10)$$

where the formulae for $w_m(\rho)$ are given in Appendix B. To find the deflections from the full support system, we simply add the deflections from each group, weighting the deflections by the fraction of the load being carried by that group. Thus

$$w(\rho,\theta) = \sum_{i=1}^{n} \epsilon_i w_i(n_i,\beta_i,\rho,\theta-\phi_i), \qquad (12)$$

where

$w(\rho,\theta)$ = plate deflection
n = number of groups or rings
ϵ_i = the fractional load carried by i^{th} ring
$\sum \epsilon_i = 1$
w_i = plate deflections with a single ring of point supports
n_i = number of support points on the i^{th} ring
β_i = radius of the i^{th} ring
ϕ_i = azimuthal offset of points on i^{th} ring

A given support system is optimized by varying the forces, radii, and rotation angles of each group to minimize the rms deflection. For the cases described below the optimization was made by numerically evaluating the rms deflection with a computer, and using a standard optimizing package for nonlinear functions. In addition, some of these results have been independently checked with a finite element analysis program. (Taylor, Asfura, and Budiansky, 1982)

A single group of support points gives an rms deflection that varies with the radius of the ring and with the number of support points on the ring. The rms deflection (or rather the support efficiency) as a function of these two parameters is shown in Figure 3. Note that as the radius of the ring approaches one, and the number of support points becomes large, that the deflections approach those of a plate simply supported along its rim. It is interesting that six points is already a very close approximation to a continuous ring. As the radius of the ring approaches zero, the deflections become those of a plate supported by a single point at its center. The deflections of the plate supported by a ring at the outer edge define a kind of "natural" scale for the deflections. The rms deflection near the optimum is shown in Figure 4 and is a factor of about 25 smaller than the natural scale. This dramatic improvement is a reflection of the fact that deflections vary as a^4. This also leads to great sensitivity to support errors. Except very near the minimum itself, the rms varies essentially linearly with the radius of the support ring.

When one analyzes supports with multiple rings of points a variety of point topologies become possible. In other words, specifying the number of support points does not provide enough information to readily optimize the support system. If one considers the mathematical character of the rms deflection function for a specified number of points, the function will have multiple extrema in general. These extrema typically exhibit different symmetries, and thus the topologies for each extrema should be found and then each used as a starting point for the optimization.

The problem of optimizing the positions and forces of N points has 3N variables and 3 constraints (net force = 1, net moments = 0). In addition rotation of the coordinate grid

about the plate center has no effect. Thus we seek the minimum value of a function in a 3N-4 dimensional space. Since this can be a very large space, and the function is nonlinear in the variables, the mathematical difficulties are enormous. We will reduce the difficulty by adding symmetry conditions whenever possible. For most cases of interest, a system of support with reflection symmetry about 3 axes is desired. This reduces the problem to $2N/3 - 1$ variables. We now divide this space into regions with distinct symmetry properties relative to the reflection axes. These can be exhibited on one sixth of the circular plate. An example of this decomposition for 18 points is shown in Figure 5. The notation uses the superscript for the number of points on the first symmetry axis, the subscript for the second symmetry axis.

Some topologies are obviously not candidates for efficient support systems. Others are, and these have been optimized with the computer. The number of local minima for each topology is believed to be very small, probably one in many cases. When multiple minima exist, we are not certain that the lowest minimum has been found, but expect that this is the case.

We have found that the topologies that produce the lowest extrema (smallest rms deflection) are those approximating a triangular grid, as we would expect from the discussion on infinite plates. As the number of support points grows, the number of possible topologies grows as well, and for large numbers of support points selecting the best topology may be a difficult task. We have found in fact that several topologies may have essentially identical support efficiencies. Particularly for circular plates and some values of N, the triangular grid may not always provide an obvious natural topology. For example, for $N = 9$, the triangular grid is unsuitable and the support is quite inefficient. We know that no support system can have an efficiency factor better than that of the infinite triangular grid. Thus, in practice the efficiency of a given optimized topology can be compared to the triangular grid and an upper bound on the possible improvement by choosing another topology can be assessed.

A variety of supports have been optimized. For these cases we have assumed $\nu = 0.25$. The simplest cases are shown in Figure 6, indicating the number and location of the support points, and the alternate topologies considered. Contour plots of the plate deflections for these cases are shown in Figure 7. The actual optimum parameters are given in Table 1 which gives the number of support points, the number of parameters optimized, the ring radii, the forces for each ring of supports, the azimuthal rotation for each ring of supports, the achieved efficiency (from which the rms deflection for a given case can readily be found using Equation 4), and the ratio of the peak-to-valley deflection to the rms deflection. The efficiency coefficients found are also plotted in Figures 15 and 16 along with the efficiency functions for the three infinite plate support geometries. We now give brief descriptions of the support systems.

The single support point system has no parameters to be optimized, and has rms deflections some 2.2 times greater than the limit suggested by the infinite triangular grid. The two point system has a radius that can be varied, and when optimized, this system gives an efficiency function that is 7.2 times the limit. The three point support is the most common of support systems, and its optimum occurs at the well known radius of $\beta = 0.645$. It is somewhat surprising (and disappointing) that the best three point efficiency is 4.8 times the limit. Continuing on the single ring cases, we see that a six point system is optimized for $\beta = 0.683$ and has an efficiency 2.5 times the limit. Adding more points to a single ring now becomes less efficient than creating new rings of support points. The simplest addition is a new ring with zero radius, a point at the center. This form of seven point support system is noticeably more efficient than the six point system, as is seen in Figure 16. This naturally raises the question whether a six point system with one point at the center surrounded by five points can be more efficient than the conventional single ring six point system. Optimization reveals that the single 6 point ring is better by about 13%.

Full three ring systems are needed when we move to nine point supports. Here symmetry allows the two topologies shown in Figure 8. Both have almost identical efficiencies. Note that the nine point systems have much lower efficiency than the six or seven point supports. It can be explained as due to the fact that "complete" triangular grids cannot be made with nine points.

A complete triangular grid can be made with 12 points and the results for the best topology are given in Table 1. The topologies and locations of the optimized points are shown in Figure 9. The best two, 12_1^1 and 12_0^2, have essentially the same efficiency. As expected, the triangular grid gives superior performance, with an efficiency about 1.6 times worse than the infinite triangular grid. Optimized 15 point systems are shown in Figure 10. Topologies 15_1^2 and 15_0^1 are about equal, but since no triangular grid configuration is possible, the efficiency is poor.

Moving up to the next complete triangular grid we find the 18 point system (we omit the central point). Several topologies give equivalent efficiencies (18_0^0, 18_1^1, and 18_2^2), indicating that strict triangular grid topologies are not essential, and the circular nature of the plate is more important. Several optimized topologies are shown in Figure 11. Contour maps of the deflections are shown in Figure 12. Actually completing the grid by adding the 19th point at the center gives an even higher efficiency as is seen in Figures 15 and 16.

As we increase the number of support points, it probably becomes less important to choose numbers of support points consistent with triangular grids. The next triangular grid system has 27 support points, with an optimum efficiency about 1.4 times that of the infinite triangular grid. Several optimized topologies are shown in Figure 13. Quite similar efficiencies are found for 27_0^3 and 27_1^2.

We complete our examples of discrete supports with a 36 point support system. The 200" telescope primary has a 36 point support system, and the proposed support system for the individual mirror segments of the University of California Ten Meter Telescope has this number of supports. There are 28 different topologies that satisfy the stated symmetry conditions. The best candidates have been optimized,and the support point locations are shown in Figure 14. As usual, several systems (36_0^0, 36_1^1, 36_3^3) are equally efficient. The optimized support efficiency is only about 40% worse than that of the infinite triangular grid.

When so many support points are used, the system is so complex that a variety of similar support positions gives similar results. For example, if one assumes that all 36 points must lie on three rings of 6, 12, and 18 points, one greatly reduces the number of variables, but the final optimum is only about 15% worse than the fully optimized system. This does not mean that one can achieve this theoretical performance without great care. On the contrary, as one goes to more and more supports, the care and detail in the analysis required to achieve the optimum goes up dramatically. Quite minor changes in the parameters can lead to large changes in the deflections. Considered in the abstract, however, it does seem to be the case that the multiple dimensional space in which one searches for the minimum does have rather flat "valleys" where more than one set of parameters will give rather similar rms deflections. Even so, the walls of these

"valleys" are exceedingly steep, and great care is needed to achieve the performance indicated here.

Based on our experience with the supports analyzed here, it appears likely that if one goes to even more support points, concentric rings of point supports are an adequate approximation to the ideal, but more complex optimum geometry. The most efficient use of support points in this situation is likely to be one with the number of supports per ring increasing outwards in the series 6, 12, 18, 24, etc. As noted before, the degree to which one has optimized the use of the support points can be checked by comparing the efficiency coefficient against that of an infinite triangular grid. For a well-designed system, as the number of support points becomes large, the edge effects become negligible, and the efficiency coefficient should equal that of the infinite plate.

Another way to evaluate the quality of the point support systems is to compare them with special cases having an infinite number of support points on each ring. Thus we turn to the analysis of continuous ring supports. These are noticeably simpler to analyze and optimize than discrete point supports, since the number of parameters for optimization is smaller and the actual analytic expressions for the deflections are substantially simpler. One again uses the principle of superposition, and uses the formula for a ring support as given in Appendix B. Since the number of support points is not defined, we return to the notation of Equation 3 and study the parameter ξ as a function of the number and radii of the ring supports. As with points, we do not insist that the deflections vanish at the rings but rather let the deflections at the rings be determined from the elastic equations governing the plate deflections.

We have optimized the radius and force for each ring, and the results are shown in Figure 15. We have also included the theoretical limits for the three infinite plate cases, and some of the optimized point support systems in this figure.

It is interesting to use this graph to compare a ring system's efficiency against the point support system efficiencies. For example, notice that the deflection achievable from three continuous rings is only slightly better than that achieved with three "rings" of discrete support points as seen in the 36 point support system. This provides confirmation for the idea that adding more points to a given ring is not productive beyond a certain point, and that one benefits much more by adding new rings of support points.

The support point efficiency is shown in Figure 16. As expected, as the number of support points grows, the efficiency approaches that of a triangular grid.

5. Sensitivity of Deflections to Support Perturbations

In the preceding discussion, we have given the theoretical limits for plate deflections that can be achieved. In practice, various approximations, simplifications, and fabrication or alignment errors will degrade the performance of the support system. Particularly when the number of supports is large, the necessary superposition of the deflections associated with each support point that will allow almost perfect cancellations of these deflections becomes a very delicate procedure.

When one is supporting a single curved mirror, maintaining the exact radius of curvature is not always critical, and in this case, some relaxation of the tolerances is often possible, since the first order effect introduced by analysis errors, etc., is typically a change in the curvature of the plate. One is fortunate when this can be focused out. For cases where an optical flat is being supported,, or when a series of segments are being supported that must have identical radii of curvature, any error in the mirror shape becomes critical.

If we assume that the optimum support is known, the effect of displacements of the supports (in the plane of the mirror) from their optimum location can be understood by the following. The displacement of a point is equivalent to the support force being in the correct position plus a moment being applied at the support point with a size equal to the product of the force at that point times the displacement of the support point. The superposition of the resulting deflections from each of the support point errors gives the additional surface error introduced by the support deflections.

Perturbations of support positions and forces must satisfy the constraints of overall equilibrium; the sum of the forces equals the weight of the mirror, and the net moments about the mirror center must vanish.

The true optimization of a support system is an extremely painstaking procedure. However, we conjecture on the basis of several numerical èxperiments, that the exact support positions can be adjusted over a small range without grossly increasing the deflections, as long as one carefully optimizes the forces applied at those points. Fortunately, the mathematical optimization of the forces is a linear problem, hence a unique optimum exists. It can be easily found if the deflection for each group of support points (evaluated as sole supports) is known. As indicated earlier, the deflections at the support points will not necessarily vanish, but will follow from the analysis. An example showing two configurations of the same topology is shown in Figure 17. These have essentially identical efficiencies.

6. Conclusions

We have described the general concepts, general scaling laws, and given some specific examples (infinite plates and circular plates) for supporting thin plates on a number discrete points. These descriptions can serve as the basis for beginning the design of support systems for thin telescope mirrors. In addition they provide a basis for evaluating the relative efficiency of a given system. For any real mirror support system, an analysis that includes the detailed shape (non-circular geometry, central holes, etc.) and the curvature is essential. A careful examination of tolerances, although difficult, is also invaluable.

Acknowledgments

We thank Michael Budiansky, Alex Asfura, Robert Taylor, Karl Pister, and Enzo Ciampi for their excellent counsel and aid with the computing. We gratefully appreciate the work of Barbara Schaefer on the illustrations.

References

Couder, A. *Research on the Deformations of Large Mirrors Used For Astronomical Observations* Bulletin Astronomique VII (1931) Memoires Et Varietes p. 201 ff (translated by E. T. Pearson)

Crawford, D. L., Meinel, A. B. , and Stockton, M. W. *Support and Testing of Large Astronomical Mirrors.* Symposium Proceedings (Tucson, Arizona, 1968) Optical Sciences Center Technical Report # 30

Medwadowski, S. , (1981) private communication

Pearson, E., *Optical and Infrared Telescopes for the 1990's* Kitt Peak National Observatory Conference Proceedings (1980)

Taylor, R. , Asfura, A., and Budiansky, M., (1982) private communication

Timoshenko, S. and Woinowsky-Krieger, S., *Theory of Plates and Shells.* Second edition (1959)

Appendix A

Deflections of Semi-Infinite Plates Supported on Many Support Points

The question of efficiency of support of a large plate can be addressed by determining the root mean square deviation of the deflection from the mean deflection. Since the plates are assumed to be very large, with many support points, edge effects can be neglected. Consequently, the best support distribution of points will be among the class of geometries where all support points look alike.

There are three geometries that are possible. If we consider a given point, it can have either 3, 4, or 6 nearest neighboring points. No other distribution of points will have the symmetry that all points look alike. These three topologies are shown in Figure 1.

We now wish to calculate the deflections of a plate supported by each of these three support types. Since we are interested in the support efficiency, we must arrange the support spacing so that the area carried by each support point is the same in all three cases. In this way, we can directly compare the deflections.

The deflections of a rectangular grid of support points with spacings of a and b are described by Timoshenko and Woinowsky-Krieger (1959), so the deflections for the case of four neighboring support points can be readily found.

$$D_{rectangle}(a,b;x,y) = \frac{qb^4}{384D}\left(1-\frac{4y^2}{b^2}\right)^2 + A_0 + \frac{qa^3b}{2\pi^3 D}\sum_{m=2,4,6\ldots}^{\infty}\frac{(-1)^{m/2}\cos\frac{m\pi x}{a}}{m^3\sinh\alpha_m\tanh\alpha_m}\left[(\tanh\alpha_m)\frac{m\pi y}{a}\sinh\frac{m\pi y}{a}-(\alpha_m+\tanh\alpha_m)\cosh\frac{m\pi y}{a}\right]$$

where

$$A_0 = -\frac{qa^3b}{2\pi^3 D}\sum_{m=2,4,6\ldots}^{\infty}\frac{1}{m^3}\left(\alpha_m-\frac{\alpha_m+\tanh\alpha_m}{\tanh^2\alpha_m}\right)$$

and

$$\alpha_m = \frac{m\pi b}{2a}$$

Setting $a = b$ gives the square grid case.

The deflections for the six point case (a triangular grid) can be found by using the principle of superposition. An elegant solution for this problem was obtained by S. J. Medwadowski (1981) using the superposition of two different plate support configurations. We present here a somewhat simpler solution based on the same idea. Consider the geometry shown in Figure A1. We can write the deflections as the sum of the deflections of a rectangular grid of supports and the deflections of a displaced rectangular grid of supports.

If we assume the spacing of the triangular grid is b, and assume the rectangular grid has a spacing of a and b, we can write the rectangular grid deflections as

$$D_{rectangle}(a,b;x,y) \quad with \quad a = \sqrt{3}\,b,$$

The triangular grid will then give deflections of

$$D_{triangle}(b,x,y) = \frac{1}{2}D_{rectangle}(a,b;x,y) + \frac{1}{2}D_{rectangle}(a,b;x-\frac{a}{2},y-\frac{b}{2}).$$

The three point support system can be handled in a similar way. Figure A2 shows the hexagonal grid of supports. Assuming the point separation is b, one can write the deflections as the sum of four displaced rectangular deflections as is indicated in the figure. We then obtain for the hexagonal grid, deflections of

$$D_{hexagon}(b;x,y) = \frac{1}{4}\Big[D_{rectangle}(\alpha,\beta;x,y) + D_{rectangle}(\alpha,\beta;x-\frac{\alpha}{2},y-\frac{\beta}{2}) + D_{rectangle}(\alpha,\beta;x-\gamma,y) + D_{rectangle}(\alpha,\beta;x-\frac{b}{2},y-\frac{\beta}{2})\Big]$$

where

$$\alpha = 3b, \qquad \beta = \sqrt{3}b, \quad \text{and} \qquad \gamma = -b.$$

Note that for these cases, the areas per point are:

$$A_{triangle} = \frac{\sqrt{3}}{2}b^2$$
$$A_{square} = b^2$$
$$A_{hexagon} = 3\frac{\sqrt{3}}{4}b^2.$$

We write the solution in the form

$$\delta = \gamma\frac{q}{D}\left(\frac{A}{N}\right)^2.$$

where q = the applied pressure on the plate,
D = the modulus of rigidity of the plate,
$\frac{A}{N}$ = the plate area per support point.

We can define δ as either the peak deflection, the mean deflection, or the root mean square deviation of the deflection from the mean. For each of these we can compare the relative efficiencies of the three configurations. Values of γ (x 10^3) are given for each of the definitions and configurations in the following table.

configuration	peak	mean	rms
triangular	4.95	3.71	1.19
square	5.80	3.87	1.33
hexagonal	9.70	4.70	2.36

Appendix B

Deflections of a Circular Plate on a Ring of Point Supports

The deflections of thin, constant thickness plates are of great interest in optical support systems. Many problems can be solved by the appropriate superpositions of solutions of the case of a circular plate axially supported by a single concentric ring of point supports (as shown in Figure 2). We derive here the solution to this problem.

Assume a uniformly loaded plate of radius a and stiffness D, with total load P, is supported by k point supports located at $r = b\ (=\beta a)$ and $\theta = 2j\pi/k$, $j = 1, \ldots k$. The deflection $w(r,\theta)$ is governed by

$$D\nabla^4 w = -\frac{P}{\pi a^2} + \frac{P}{k}\sum_{j=1}^{k}\frac{\delta(r-b)}{b}\delta\left(\theta - \frac{2j\pi}{k}\right). \tag{1}$$

The Fourier series for $\sum_{j=1}^{k}\delta\left(\theta-\frac{2j\pi}{k}\right)$ is of the form

$$\frac{a_0}{2} + \sum_{m=1}^{\infty} a_m \cos km\theta,$$

with

$$a_m = \frac{1}{\pi}\sum_{j=1}^{k}\int_0^{2\pi}\delta\left(\theta-\frac{2j\pi}{k}\right)\cos km\theta\, d\theta = \frac{k}{\pi},$$

hence the loading is

$$-\frac{P}{\pi a^2} + \frac{P}{2\pi b}\delta(r-b) + \frac{P}{\pi}\frac{\delta(r-b)}{b}\sum_{m=1}^{\infty}\cos km\theta.$$

Assume the deflection has the form

$$w(r,\theta) = \sum_{m=0}^{\infty} w_m(r)\cos km\theta, \tag{2}$$

where w_0 is governed by

$$\frac{1}{r}\frac{d}{dr}\left\{r\frac{r}{dr}\left[\frac{1}{r}\frac{d}{dr}\left(r\frac{dw_0}{dr}\right)\right]\right\} = -\frac{P}{\pi a^2} + \frac{P}{2\pi b}\delta(r-b),$$

i.e., w_0 is just the deflection of a plate supported on a ring of radius b. We can obtain w_0 by superposing the deflections of simply supported plates that are uniformly loaded and ring-loaded, with total loads equal and opposite, to obtain

$$\frac{8\pi D}{Pa^2}w_0(\rho) = \frac{1-\beta^2}{2}\left[\frac{(3+\nu)-(1-\nu)\rho^2}{1+\nu}\right] - \frac{1-\rho^2}{8}\left[\frac{5+\nu}{1+\nu}-\rho^2\right] + (\beta^2+\rho^2)\ln\beta, \quad \rho < \beta$$
$$= \frac{(1-\rho^2)}{8}\left[\frac{(7+3\nu)-4(1-\nu)\beta^2}{1+\nu}+\rho^2\right] + (\beta^2+\rho^2)\ln\rho, \quad \rho > \beta. \tag{3}$$

For $m \geq 1$, we have

$$\left(\frac{d^2}{dr^2}+\frac{1}{r}\frac{d}{dr}-\frac{k^2m^2}{r^2}\right)^2 w_m = \frac{P}{\pi bD}\delta(r-b).$$

In other words,

$$\left(\frac{d^2}{dr^2}+\frac{1}{r}\frac{d}{dr}-\frac{k^2m^2}{r^2}\right)^2 w_m = 0, \quad r \neq b. \tag{4}$$

If we define $w_m^{(a)}$ and $w_m^{(b)}$ as the restrictions of w_m to $(b,a]$ and $[0,b)$, respectively, then we have the continuity equations

$$w_m^{(a)}(b+) = w_m^{(b)}(b-), \tag{5}$$
$$\frac{d}{dr} w_m^{(a)}(b+) = \frac{d}{dr} w_m^{(b)}(b-),$$
$$\frac{d^2}{dr^2} w_m^{(a)}(b+) = \frac{d^2}{dr^2} w_m^{(b)}(b-),$$
$$\frac{d^3}{dr^3} w_m^{(a)}(b+) - \frac{d^3}{dr^3} w_m^{(b)}(b-) = \frac{P}{\pi b D}.$$

The solution takes the form (with $n = km$)

$$w_m^{(a)}(r) = A_m r^n + B_m r^{n+2} + C_m r^{-n} + D_m r^{-n+2}, \tag{6}$$
$$w_m^{(b)}(r) = A'_m r^n + B'_m r^{n+2},$$

and the continuity equations become

$$(A_m - A'_m) b^n + (B_m - B'_m) b^{n+2} + C_m b^{-n} + D_m b^{-n+2} = 0 \tag{7}$$
$$n(A_m - A'_m) b^n + (n+2)(B_m - B'_m) b^{n+2} - nC_m b^{-n} - (n-2) D_m b^{-n+2} = 0$$
$$n(n-1)(A_m - A'_m) b^n + (n+2)(n+1)(B_m - B'_m) b^{n+2} + n(n+1) C_m b^{-n} + (n-2)(n-1) D_m b^{-n+2} = 0$$
$$n(n-1)(n-2)(A_m - A'_m) b^n + (n+2)(n+1) n (B_m - B'_m) b^{n+2} - n(n+1)(n+2) C_m b^{-n} - n(n-1)(n-2) D_m b^{-n+2} = \frac{Pb^2}{\pi D}$$

The solutions are

$$(A_m - A'_m) b^n = -\frac{1}{n(n-1)} \frac{Pb^2}{8\pi D}, \tag{8}$$
$$(B_m - B'_m) b^{n+2} = \frac{1}{n(n+1)} \frac{Pb^2}{8\pi D},$$
$$C_m b^{-n} = -\frac{1}{n(n+1)} \frac{Pb^2}{8\pi D},$$
$$D_m b^{-n+2} = \frac{1}{n(n-1)} \frac{Pb^2}{8\pi D}.$$

In addition, $w_m^{(a)}$ must satisfy the conditions of zero moment and shear at $r = a$. Now, using standard expressions,

$$\frac{1}{D} M_r = \left[\frac{\partial^2 w}{\partial r^2} + \nu \left(\frac{1}{r} \frac{\partial w}{\partial r} + \frac{1}{r^2} \frac{\partial^2 w}{\partial \theta^2} \right) \right]_{r=a} = 0, \tag{9}$$

so

$$\frac{d^2}{dr^2} w_m(a) + \nu \left[\frac{1}{a} \frac{d}{dr} w_m(a) - \frac{n^2}{r^2} w_m(a) \right] = 0; \tag{10}$$

furthermore

$$\frac{1}{D} M_{r\theta} = (1-\nu) \frac{1}{r} \frac{\partial}{\partial \theta} \left(\frac{\partial w}{\partial r} - \frac{w}{r} \right), \tag{11}$$
$$-\frac{1}{D} Q_r = \frac{\partial}{\partial r} \left(\frac{\partial^2 w}{\partial r^2} + \frac{1}{r} \frac{\partial w}{\partial r} + \frac{1}{r^2} \frac{\partial^2 w}{\partial \theta^2} \right),$$

and

$$-\frac{1}{D} V_r = \left[\left(-\frac{1}{D} Q_r + \frac{1}{r} \frac{\partial M_{r\theta}}{\partial \theta} \right) \right]_{r=a} \tag{12}$$
$$= \left[\frac{\partial}{\partial r} \left(\frac{\partial^2 w}{\partial r^2} + \frac{1}{r} \frac{\partial w}{\partial r} + \frac{1}{r^2} \frac{\partial^2 w}{\partial \theta^2} \right) + (1-\nu) \frac{\partial^2}{\partial \theta^2} \left(\frac{1}{r^2} \frac{\partial w}{\partial r} - \frac{w}{r^3} \right) \right]_{r=a}$$

so that

$$\left[\frac{d}{dr} \left(\frac{d^2}{dr^2} w_m^{(a)} + \frac{1}{r} \frac{d}{dr} w_m^{(a)} - \frac{n^2}{r^2} w_m^{(a)} \right) - n^2 (1-\nu) \left(\frac{1}{r^2} \frac{d}{dr} w_m^{(a)} - \frac{w_m^{(a)}}{r^3} \right) \right]_{r=a} = 0 . \tag{13}$$

Substituting (6) into (10) and (13), we see that A_m, B_m, C_m, D_m must satisfy

$$(1-\nu) n(n-1) A_m a^n + (n+1)[n+2-\nu(n-2)] B_n a^{n+2} + (1-\nu) n(n+1) C_m a^{-n} + (n-1)[n-2-\nu(n+2)] D_m a^{-n+2} = 0, \tag{14}$$

$$(1-\nu) n^2 (n-1) A_m a^n + n(n+1)(n-4-\nu n) B_m a^{n+2} - (1-\nu) n^2 (n+1) C_m a^{-n} - n(n-1)(n+4-\nu n) D_m a^{-n+2} = 0.$$

Since C_m and D_m are known already from (8) we can solve for A_m and B_m:

$$A_m a^n = \frac{Pa^2}{8\pi D} \frac{\beta^n}{3+\nu} \left[(1-\nu) \left(\frac{1}{n-1} - \frac{\beta^2}{n} \right) + \frac{8(1+\nu)}{n^2 (n-1)(1-\nu)} \right],$$
$$B_m a^{n+2} = -\frac{Pa^2}{8\pi D} \frac{\beta^n}{3+\nu} (1-\nu) \left(\frac{1}{n} - \frac{\beta^2}{n+1} \right). \tag{15}$$

We rewrite the remaining solutions as

$$C_m a^{-n} = -\frac{Pa^2}{8\pi D} \frac{\beta^{n+2}}{n(n+1)}, \tag{16}$$
$$D_m a^{-n+2} = \frac{Pa^2}{8\pi D} \frac{\beta^n}{n(n-1)},$$
$$A'_m a^n = A_m a^n + \frac{Pa^2}{8\pi D} \frac{\beta^{-n+2}}{n(n-1)},$$
$$B'_m a^{n+2} = B_m a^{n+2} - \frac{Pa^2}{8\pi D} \frac{\beta^{-n}}{n(n+1)}.$$

Thus the solution to (1) has been obtained. It is given by using (15) and (16) in (6), and (6) in (2).

N	#var	$\gamma_N(\times 10^3)$	$\frac{p-p}{rms}$	n_i, β_i, ε_i, ϕ_i								
1	0	2.60	3.8									
2	1	8.56	3.9	β = .3538								
3	1	5.76	4.2	β = .645								
6_1^1	1	2.93	4.3	β = .681								
7_1^1	2	2.36	4.9	n = 1 6 β = 0 .737 ε = .1183 .8817 ϕ = 0 0								
9_1^2	5	3.76	5.0	n = 3 3 3 β = .2825 .7936 .7700 ε = .2309 .3637 .4054 ϕ = 0 0 1.0472								
12_1^1	6	1.94	5.1	n = 3 3 3 3 β = .3151 .7662 .8257 .8257 ε = .2783 .2843 .2187 .2187 ϕ = 0 1.0472 .3497 -.3497								
15_0^1	7	2.32	5.4	n = 3 3 3 3 3 β = .3192 .7765 .8412 .7765 .8412 ε = .2833 .2046 .1538 .2046 .1538 ϕ = 0 .7833 .2615 -.7833 -.2615								
18_1^1	9	1.89	5.5	n = 3 3 3 3 3 3 β = .4741 .3195 .8171 .8536 .8171 .8536 ε = .1625 .2071 .1731 .1421 .1731 .1421 ϕ = 0 1.0472 .7820 .2663 -.7820 -.2663								
27_1^2	14	1.65	5.7	n = 3 3 3 3 3 3 3 3 3 β = .2044 .8740 .4777 .5555 .8787 .8574 .5555 .8787 .8574 ε = .1152 .1049 .1347 .1162 .0955 .1110 .1162 .0955 .1110 ϕ = 0 0 1.0472 .3399 .4280 .8383 -.3399 -.4280 -.8383								
36_1^1	9	1.63	6	n = 6 6 6 6 6 6 β = .2569 .5771 .5771 .8830 .8834 .8830 ε = .1671 .1812 .1812 .1549 .1607 .1549 ϕ = 0 .2649 .7823 .1703 .5236 .8769								

TABLE 1

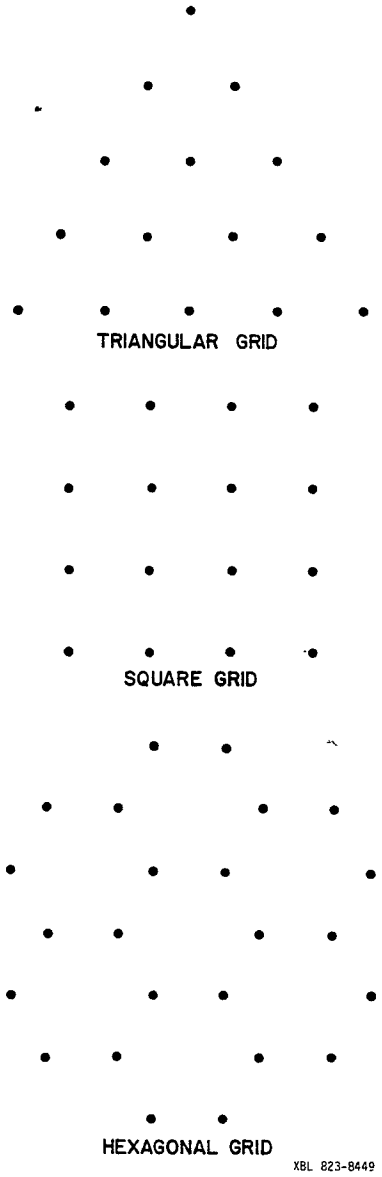

1. The three kinds of point symmetric infinite grids. These grids are shown with equal areas per point. As described in the text, the triangular grid is the most efficient.

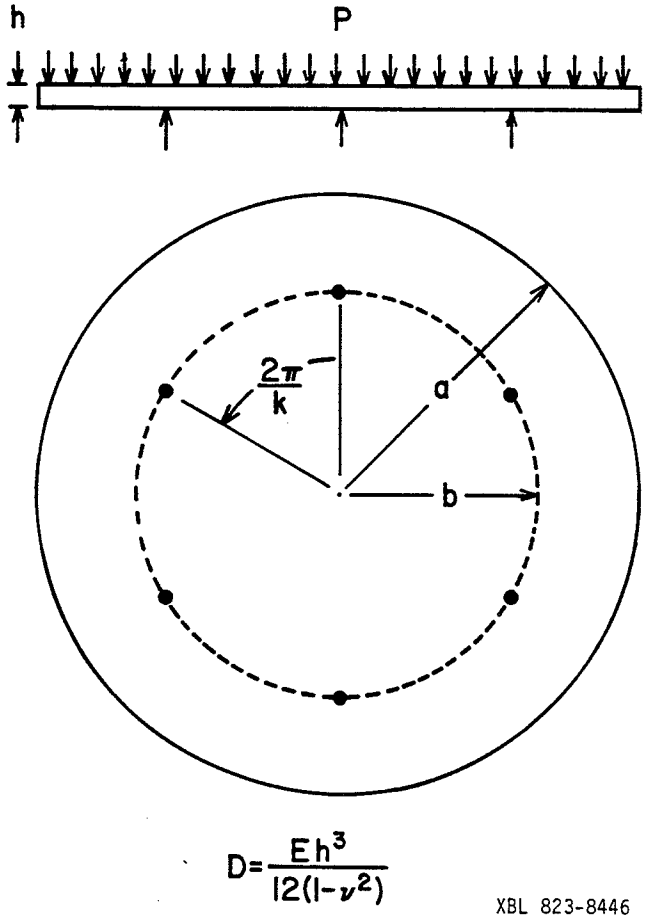

2. The geometry and notation for supporting a circular plate on a single ring of support points. P is the applied force. In the figure six support points are used.

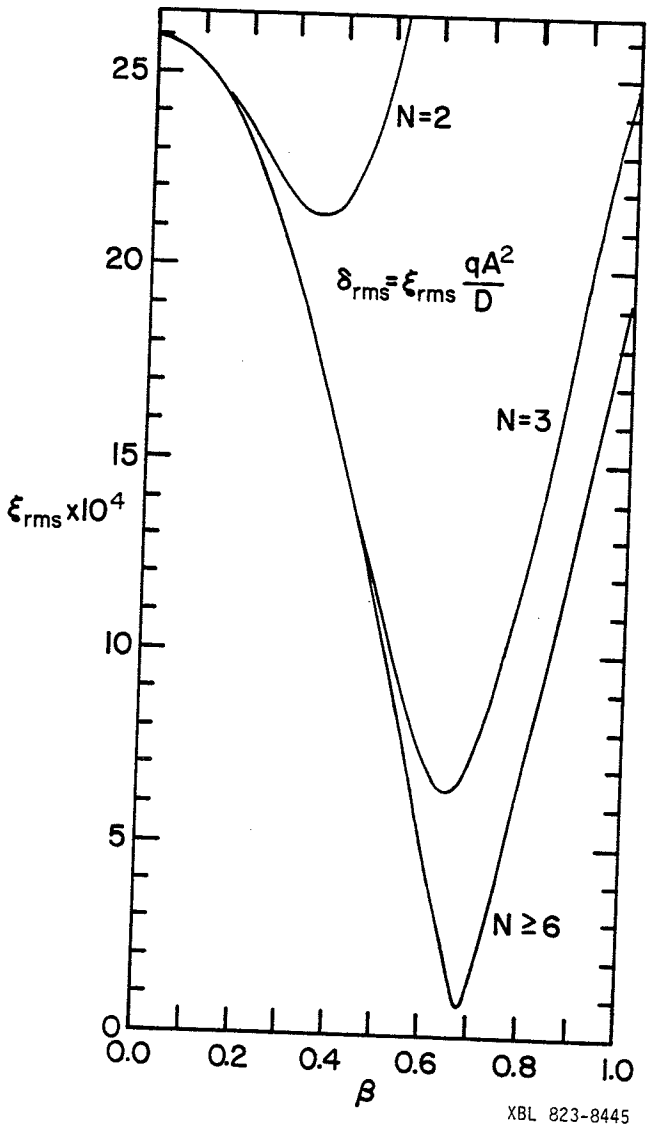

3. The support efficiency as a function of the ring radius for points on a single ring. Cases with 2, 3, and 6 support points are shown. More than 6 points is indistinguishable from 6 points. Note the dramatic improvement with increasing N, and the great sensitivity of the efficiency with the normalized radius β.

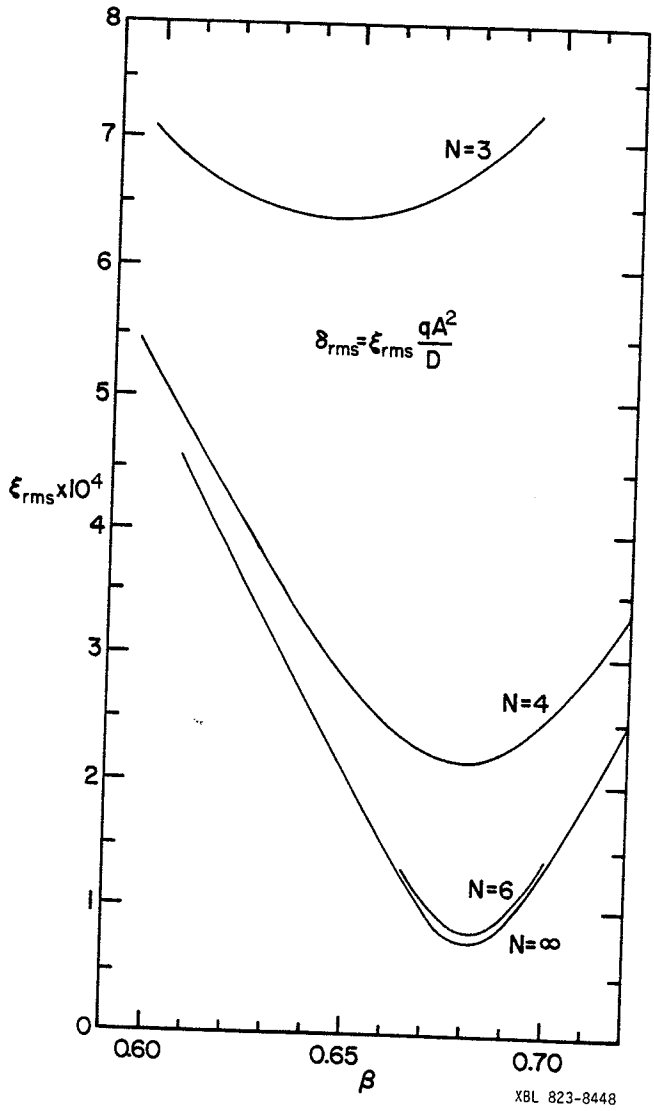

4. The region of Figure 3 near the minimum is expanded for clarity. Note again the small difference between N = 6 and N = infinity.

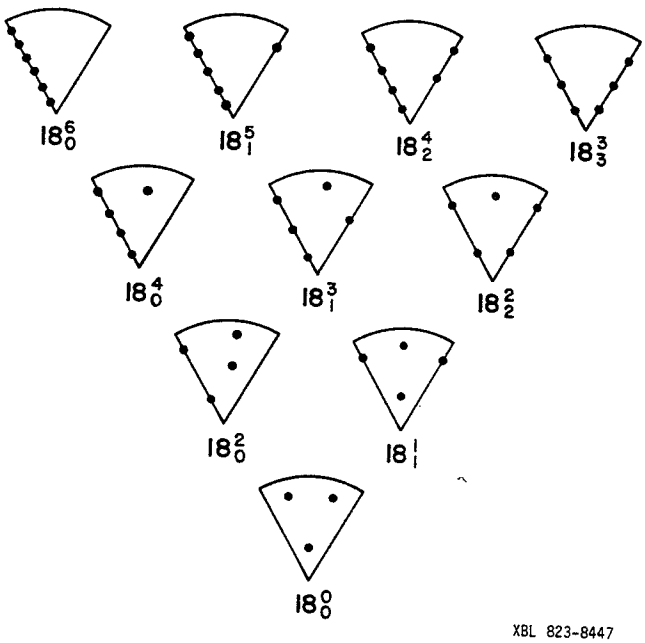

5. The possible support topologies for an 18 point support. Three fold reflection symmetry of the support system is assumed in establishing the possible topologies. The nomenclature gives in the superscript the number of points on one axis of symmetry and the subscript gives the number of points on the other axis.

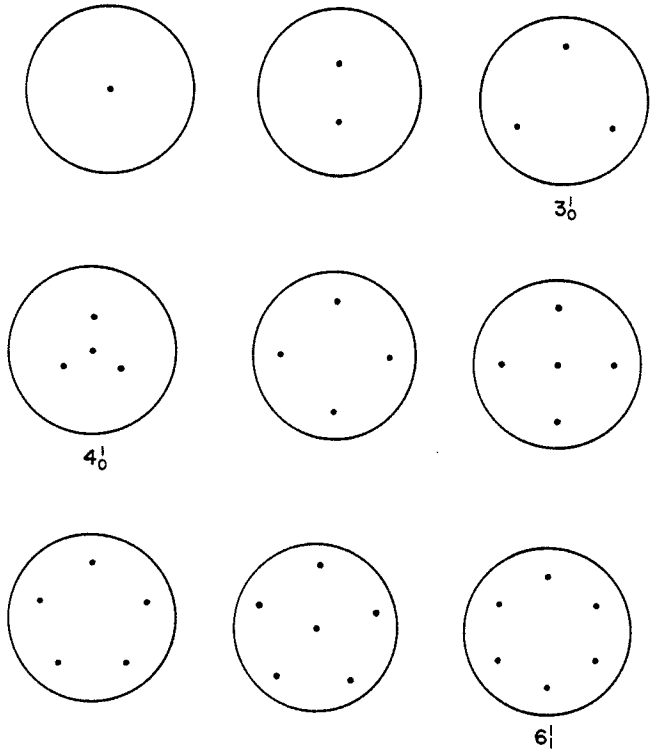

6. The optimal locations of support points are given for the general support configurations shown. Note that the 4_0^1 case has a negative force applied to the central point. The plots are ordered in the sense of increasing efficiency.

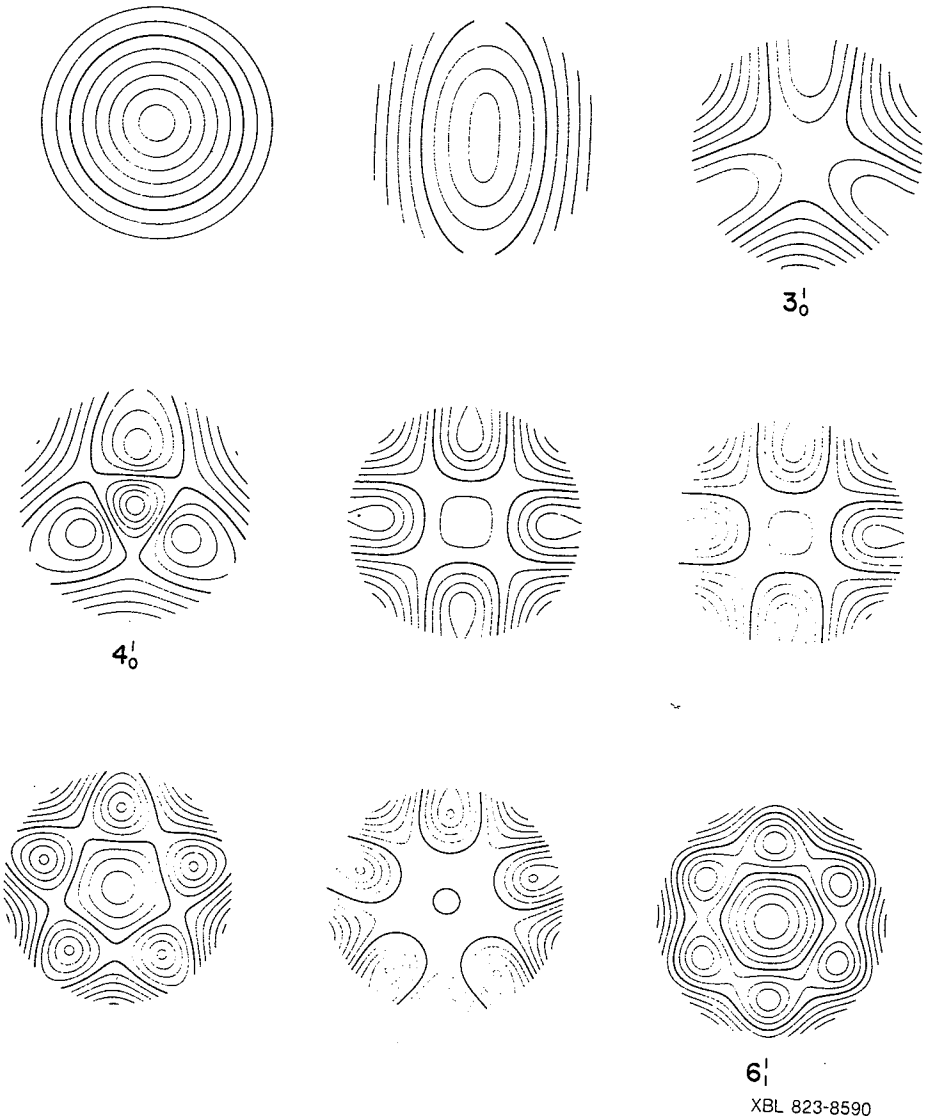

7. Contour maps of the deflections for the support configurations of Figure 6. The contour interval for each plot is one half times the rms deflection of the surface from the mean deflection. The heavy line is the mean deflection.